Statistical Analyses and Theoretical Models of Single-Molecule Enzymatic Dynamics

Gregory K. Schenter* and H. Peter Lu

William R. Wiley Environmental Molecular Sciences Laboratory, Pacific Northwest National Laboratory, P.O. Box 999, Richland, Washington 99352

X. Sunney Xie*

Department of Chemistry and Chemical Biology, Harvard University, 12 Oxford Street, Cambridge, Massachusetts 02138

Received: July 12, 1999; In Final Form: October 5, 1999

Real-time observation of enzymatic turnovers of single molecules has revealed non-Markovian dynamical behavior. Although chemical kinetics (such as the Michaelis−Menten mechanism) are sufficient to describe the average behavior of an ensemble of molecules, statistical analysis of the single-molecule fluorescence time trace reveals fluctuations in the rate of the activation step. These fluctuations are attributed to slow fluctuations of protein conformations. In this paper, we discuss models of the dynamical disorder behavior and relate them to observables of single molecule experiments. Simulations based on a discrete multistate model and a diffusive model are compared with experiment data. The role of various correlation functions, including higher order time correlation functions, in the interpretation of the underlying dynamics is discussed.

Introduction

Recent advances in single-molecule spectroscopy have spurred much research on the dynamical behavior of single molecules.[1−4] Chemical dynamics can now be probed on a single-molecule basis. For example, enzymatic turnovers of single cholesterol oxidase molecules have been observed in real time by monitoring the emission from the enzyme's fluorescent active site, flavin adenine dinucleotide (FAD).[5] Chemical kinetics (such as the Michaelis−Menten mechanism), can account for the ensemble-averaged behaviors; however, statistical analyses of the single-molecule trajectories reveal fluctuations in the rate of the activation step of the reaction. This dynamic disorder behavior is beyond the scope of conventional chemical kinetics and originates from slow fluctuations of protein conformations.[5] Ensemble-averaged experiments would not distinguish this dynamic variation of reaction rates from static heterogeneity. In this work, we present theoretical models for statistical analyses of single-molecule enzymatic dynamics. In this section, we give an overview of recent theoretical work relevant to single-molecule analyses.

Skinner and co-workers[6,7] have conducted statistical analyses of single-molecule spectral trajectories in order to understand a pioneering experiment on single-molecule spectral diffusion at cryogenic temperatures.[8] The underlying dynamics of that system is tunneling of two-level systems, which was described by a two-state jump model,[6−7] and analyzed with autocorrelation functions of the transition frequency. Silbey and co-workers[9] and Klafter and co-workers[10] have also pursued this stochastic approach to two-level systems.

Prompted by the room-temperature observations of double exponential fluorescence decays of single dye molecules in DNA complexes,[11,12] Geva and Skinner recast a two-state jump model in terms of population distributions as a function of data collection times.[13] Similar to "motional narrowing" in molecular spectroscopy,[14] this approach allowed the extraction of the time scale of conformational transitions of the systems. The two-state jumping model is within the framework of a simple reversible kinetic scheme; a more sophisticated two-state jumping model involving non-Markovian dynamics has also appeared.[15]

Of particular interest is the chemical dynamics of single molecules. The first experimental effort in this area was the ion channels studied by single channel recording.[16] There has been a large body of work on statistical analyses of the single-channel trajectories.[17] Most of the work has been in the framework of chemical kinetics, analyzing the histograms of the on- and off-periods of the ion channels. The usefulness correlation functions have not yet been explored on these systems. Yet these early works began the discussion of chemical kinetics in terms of Poisson statistics of single-molecules, which is key to the understanding of single molecule experiments.

Wang and Wolynes[18] first discussed the role of analyses of single-molecule trajectories in understanding chemical dynamics (as opposed to chemical kinetics). Slow fluctuation of the environment causing the fluctuation of the rate coefficient (which is no longer constant) results in deviations from Poisson statistics. A single-molecule experiment would be expected to show non-Poisson effects causing reaction events to "bunch up," an effect called "intermittency".[18,19] Wang and Wolynes pointed out that when such non-Poisson statistics are observed and the first-order moment of the probability is not enough to characterize the system, higher order moments contain more information. Intermittency ratios—defined as the ratio of the average of an *n*th-order moment compared to the average of a first-order moment raised to the *n*th power—have been formulated to characterize the non-Poisson behavior.[18]

The non-Poisson statistics resulting from the fluctuating rate coefficient is related to "dynamical disorder," a subject reviewed by Zwanzig.[20] The rate coefficient itself can be viewed as dependent on a stochastic control variable (such as barrier height). A time-dependent rate coefficient can be described in two ways: in terms of the control variables jumping between

10.1021/jp992324j CCC: $18.00 © 1999 American Chemical Society
Published on Web 11/13/1999

discrete values according to simple kinetics or in terms of a continuum of states undergoing diffusive changes according to a Langevin equation. For the former, transitions of the control variable are described by a master equation for the probability that the control variable has a specific discrete value. For the latter, a Langevin equation characterized by a decay rate and fluctuation amplitude describes the time dependence of control variables. The probability distribution for the control variable obeys the Fokker−Planck equation. Agmon and Hopfield first introduced this latter approach in the context the ligand rebinding in myoglobin where the rate constant depends on a protein coordinate described by the Brownian motion of a harmonic oscillator.[21] Sumi and Marcus took a similar approach to electron-transfer reactions,[22] and Bagchi, Oxtoby, and Fleming had a similar treatment for barrierless reactions in solution.[23]

In the above approach, the dynamical variable of the Langevin equation is the rate coefficient or its control variable rather than the nuclear coordinates whose variations ultimately cause the rate fluctuation. In contrast, rate theories of chemical reactions in solution take nuclear (reaction) coordinates as the dynamical variables of the Langevin equation as in Kramer's theory,[24] or the generalized Langevin equation,[25−28] as in the Grote−Hynes theory.[29] These rate theories give constant rate coefficients because the fluctuations of the nuclear coordinates occur at a much faster time scale than that of the chemical reactions.

Molecular dynamics (MD) simulations of biomolecules[30,31] are single-molecule "experiments" whose trajectory analyses have yielded detailed information of molecular interactions and their influence on chemical reactions. Wilson, Hynes, and coworkers have pioneered MD simulations of solution phase chemical reactions.[32] Neria and Karplus have done MD simulation of triosephosphate isomerase and shown that small structural changes have large effects on the rate enhancement.[33] The MD trajectories allowed them to obtain the transmission coefficient correction to transition state theory. Also, Chandler and coworkers have performed a MD simulation of a photosynthetic reaction center.[34] The trajectory of the donor and acceptor energy gap illustrated the dynamical disorder in rate on a single molecule. Unfortunately, because of practical restrictions, the single-molecule experiments have been limited to a much longer time scale (milliseconds to tens of min), preventing direct comparison of MD and experimentally measured single-molecule trajectories.

In this paper we will recast dynamic disorder in terms of trajectory analyses relevant to single-molecule real-time experiments and compare different theoretical models with experimental results. Dynamic disorder can appear in statistical analyses of experimental observables but some analyses are more informative than others. We present simulations of various correlation functions based on different models. Finally, the simulation results are compared with experimental results. The issues of conformational dynamics and its influence on enzymatic dynamics are discussed.

Formulation

We consider a general N-state kinetic scheme for the population of state i, described by the master equation for the probability density $P_i(t)$,

$$\frac{\mathrm{d}}{\mathrm{d}t}P_i(t) = \sum_{j\neq i}[k_{ij}(t)P_j(t) - k_{ji}(t)P_i(t)] \tag{1}$$

where the rate of transition from state j to state i is $k_{ij}(t)$, and the sum spans the domain of states $i \in \{1,..., N\}$. $k_{ij}(t)$, is taken to be time dependent in general, allowing for fluctuating rate coefficients. $P_i(t)$ represents the dynamic population (or probability) of the state i at a given time t. As a jump model, the current state of the system can be viewed as a dynamical trajectory between discrete states. We then write the function $I(t)$ to represent the fact that the system is in state $I\in\{1,..., N\}$ at time t. A discrete trajectory in time, $I(t)$, will represent "microscopic" realization of the state of the system.

To analyze the statistical behavior of $I(t)$, we now consider an ensemble of trajectories of $I(t)$. We denote the conditional probability that the ensemble is in the state i at time t, assuming the ensemble is in state i_0 at earlier time t_0, by $G_{ii_0}(t,t_0)$. The dynamics of this quantity is described by

$$\frac{\mathrm{d}}{\mathrm{d}t}G_{ii_0}(t,t_0) = \sum_{j\neq i}[k_{ij}(t)G_{ji_0}(t,t_0) - k_{ji}(t)G_{ii_0}(t,t_0)] \tag{2}$$

with initial conditions

$$G_{ij}(t_0, t_0) = \delta_{ij} \tag{3}$$

The conditional probabilities satisfy the composition and completeness relations

$$\sum_{i_1} G_{i_2i_1}(t_2, t_1)G_{i_1i_0}(t_1, t_0) = G_{i_2i_0}(t_2, t_0) \tag{4}$$

and

$$\sum_{i} G_{ii_0}(t,t_0) = 1 \tag{5}$$

We will consider the statistical fluctuations of $k_{ij}(t)$, viewing them as random variables with respect to the average $\langle ... \rangle$. Because of this, the conditional probabilities $G_{ii_0}(t,t_0)$ must be viewed stochastic variables themselves, satisfying a stochastic differential equation. We will assume that the time-independent, steady-state limit exists and is given by

$$P_i^{\mathrm{eq}} = \lim_{t_0 \to -\infty} G_{ii_0}(t,t_0) \tag{6}$$

independent of i_0 and $t \geq 0$. This means that the system reaches equilibrium at and after time zero. Because of this, general averages are independent of time. For $t \geq 0$,

$$\langle A(t)\rangle = \sum_{i,i_0}\langle A_i G_{ii_0}(t,0)P_{i_0}^{\mathrm{eq}}\rangle = \sum_i \langle A_i P_i^{\mathrm{eq}}\rangle = \langle A\rangle \tag{7}$$

where A_i is a general observable corresponding to state i. General n-time correlation functions are written as

$$\langle A^{(n)}(t_n)\cdots A^{(1)}(t_1)\rangle = \sum_{i_n,\cdots,i_1,i_0} \langle A_{i_n}^{(n)} G_{i_n i_{n-1}}(t_n,t_{n-1}) A_{i_{n-1}}^{(n-1)}\cdots A_{i_2}^{(2)} G_{i_2 i_1}(t_2,t_1) A_{i_1}^{(1)} G_{i_1 i_0}(t_1, 0) P_{i_0}^{\mathrm{eq}}\rangle \tag{8}$$

with $t_n \geq t_{n-1} \geq \cdots \geq t_1 \geq 0$. In this representation, the time dependence is contained in the conditional probabilities, $G_{i,i_0}(t,t_0)$.

If the system is ergodic, we may consider a single trajectory $I(t)$. In terms of the time average of the trajectory, we write the n time correlation function as

$$\langle A^{(n)}(t_n)\cdots A^{(1)}(t_1)\rangle = \lim_{T\to\infty}\frac{1}{T}\int_0^T \mathrm{d}t' A^{(n)}_{I(t_n+t')}A^{(n-1)}_{I(t_{n-1}+t')}\cdots A^{(2)}_{I(t_2+t')}A^{(1)}_{I(t_1+t')} \quad (9)$$

In this representation, the time dependence is contained in $I(t)$.

In the single-molecule enzymatic experiment, the relevant observable is the fluorescence signal from one of many different possible states of the system. A given state is either fluorescent or not. We choose the observable A_i to be ξ_i, where $\xi_i = 1$ for fluorescence "on" states and $\xi_i = 0$ for fluorescence "off" states. The resulting fluorescence signal may be represented as $\xi(t) = \xi_{I(t)}$, since at time t, the system is in state $I(t)$. In some cases, $\xi_i = 1$ for many different states and there is no means to distinguish between these "hidden" states. Because of this, a multi-state system obeying simple kinetics can appear to describe a two-state non-Markovian system. We will expand on this point in the flowing discussion.

To consider fluctuations about the equilibrium signal, we define $\Delta\xi(t) = \xi(t) - \langle\xi\rangle$, whose second-order correlation function is given by

$$C_2(t) = \frac{\langle\Delta\xi(t)\Delta\xi(0)\rangle}{\langle\Delta\xi^2\rangle} \quad (10)$$

and

$$\langle\Delta\xi(t)\Delta\xi(0)\rangle = \sum_{i,i_0}\langle\Delta\xi_i G_{ii_0}(t,0)\Delta\xi_{i_0}P^{\mathrm{eq}}_{i_0}\rangle \quad (11)$$

with the definition, $\Delta\xi_i = \xi_i - \langle\xi\rangle$. Given a stochastic trajectory of $\xi(t) = \xi_{I(t)}$, it is possible to generate a sequence of on-time durations $\{\tau_1,\tau_2,...,\tau_m,...\}$, for $\xi(t) = 1$. From this trajectory the mean on-time $\langle\tau\rangle$ may be determined as well as the on-time autocorrelation function

$$r(m) = \frac{\langle\Delta\tau_{m+m'}\Delta\tau_{m'}\rangle}{\langle\Delta\tau^2\rangle} \quad (12)$$

where we define $\Delta\tau_m = \tau_m - \langle\tau\rangle$. A comparison of this correlation function and $C_2(t)$ will be presented in the Result section.

Higher order correlation functions might contain more information than the second-order correlation function. In general, the fourth-order correlation function is

$$C_4(t_4, t_3, t_2, t_1) = \langle\Delta\xi(t_4)\Delta\xi(t_3)\Delta\xi(t_2)\Delta\xi(t_1)\rangle/\langle\Delta\xi^4\rangle \quad (13)$$

To simplify the analyses of experimental trajectories, we assume $\tau = t_2 - t_1 = t_4 - t_3$, and $t = t_3 - t_2$, and present the $C_4(t_4, t_3, t_2, t_1)$ with two variables, τ and t,

$$C_4(\tau, t) = \frac{\langle\Delta\xi(t+2\tau)\Delta\xi(t+\tau)\Delta\xi(\tau)\Delta\xi(0)\rangle}{\langle\Delta\xi^4\rangle} \quad (14)$$

where

$$\langle\Delta\xi(t+2\tau)\Delta\xi(t+\tau)\Delta\xi(\tau)\Delta\xi(0)\rangle = \sum_{i_3,i_2,i_1,i_0}\langle\Delta\xi_{i_3}G_{i_3i_2}(t+2\tau,t+\tau)\Delta\xi_{i_2}G_{i_2i_1}(t+\tau,\tau)\times \Delta\xi_{i_1}G_{i_1i_0}(\tau,0)\Delta\xi_{i_0}P^{\mathrm{eq}}_{i_0}\rangle \quad (15)$$

The analytical solutions and numerical simulations of the above three correlation functions will be presented based on three different models.

In the case of simple kinetics, $k_{ij}(t)$ is independent of time and no longer considered a stochastic variable. The expressions for the averages are simplified considerably. For simplicity of notation, it is possible to define the matrix $\mathbf{K}$, where $K_{ij} = k_{ij}(t)$ when $i \neq j$, and $K_{ii} = -\sum_{j\neq i}k_{ji}(t)$ for the diagonal elements of $\mathbf{K}$. The equation for the conditional probability distribution becomes the matrix equation,

$$\frac{\mathrm{d}}{\mathrm{d}t}\mathbf{G}(t,t_0) = \mathbf{K}\mathbf{G}(t,t_0) \quad (16)$$

with $\mathbf{G}(t_0,t_0) = 1$. In this case, $\mathbf{G}$ is no longer a stochastic variable, and we may write $\mathbf{G}(t,t_0) = \mathrm{e}^{\mathbf{K}(t-t_0)}$. Furthermore, with $[\mathbf{P}^{\mathrm{eq}}]_i = P^{\mathrm{eq}}_i$, the vector $\mathbf{P}^{\mathrm{eq}}$ is a zero eigenvector of the matrix $\mathbf{K}$, corresponding to the equilibrium population of the kinetic scheme.

Two State 1×2 Model

We will now introduce three different kinetic models and explore the behavior of correlation functions resulting from the dynamics corresponding to the models. When ever possible we include closed-form analytical expressions for the correlation functions. In a later section we will discuss more complex models. Initially we choose simple models that have fundamentally different structures and compare the qualitative dependence of the correlation functions. The simplest model that we consider is the two-state model described by the kinetic scheme

$$n_1^{\mathrm{on}} \underset{k_{12}}{\overset{k_{21}}{\rightleftharpoons}} n_2^{\mathrm{off}} \quad (17)$$

Where n_k^{on} will denote an "on" state, $\xi_k = 1$, and n_k^{off} will denote an "off" state, $\xi_k = 0$. In this case, $\xi = \begin{pmatrix}1\\0\end{pmatrix}$ and $\mathbf{K} = \begin{pmatrix}-k_{21} & k_{12}\\ k_{21} & -k_{12}\end{pmatrix}$. It follows that

$$\mathbf{G}(t,0) = \mathrm{e}^{\mathbf{K}t} = \frac{1}{\kappa}\begin{pmatrix}k_{12}+k_{21}\mathrm{e}^{-\kappa t} & k_{12}-k_{12}\mathrm{e}^{-\kappa t}\\ k_{21}-k_{21}\mathrm{e}^{-\kappa t} & k_{21}+k_{12}\mathrm{e}^{-\kappa t}\end{pmatrix} \quad (18)$$

where $\kappa = k_{12} + k_{21}$. With $p = k_{12}/\kappa$, we have $\mathbf{P}^{\mathrm{eq}} = \begin{pmatrix}p\\1-p\end{pmatrix}$. Furthermore, $\langle\xi^n\rangle = p$ for all n and $\langle\Delta\xi^2\rangle = p - p^2$, $\langle\Delta\xi^3\rangle = p - 3p^2 + 2p^3$, and $\langle\Delta\xi^4\rangle = p - 4p^2 + 6p^3 - 3p^4$. For the correlation functions, it follows that

$$C_2(t) = \mathrm{e}^{-\kappa t} \quad (19)$$

and

$$C_4(\tau,t) = [(p^2 - 2p^3 + p^4)\mathrm{e}^{-2\kappa\tau} + (p - 5p^2 + 8p^3 - 4p^4)\mathrm{e}^{-\kappa(2\tau+t)}]/(p - 4p^2 + 6p^3 - 3p^4) \quad (20)$$

We note that $C_4(\tau,t)$ has no t dependence when the duty cycle $\langle\xi\rangle$ of the $\xi(t)$ trajectory is 50% ($p = 0.5$) because the second term vanishes. For the 1×2 model, as a Markovian scheme (constant rate coefficients), the on time correlation $r(m)$ is only a spike at zero time ($r(m) = 1$ for $m = 0$ and $r(m) = 0$ for $m > 0$).

2×2 Model

In this model we have two coupled two-state channels, represented by the four-state kinetic scheme

$$\begin{array}{ccc} n_1^{\text{on}} & \underset{k'_1}{\overset{k_1}{\rightleftharpoons}} & n_3^{\text{off}} \\ \alpha\uparrow\downarrow\beta & & \alpha\uparrow\downarrow\beta \\ n_2^{\text{on}} & \underset{k'_2}{\overset{k_2}{\rightleftharpoons}} & n_4^{\text{off}} \end{array} \tag{21}$$

The physical picture of the model is two slowly inter-converting conformational states of the reactant that have different activation barriers.[35] Initially, to limit the number of parameters defining the model and to allow an analytic solution, we consider the special case where $\beta = \alpha$, $k'_1 = k_1$, and $k'_2 = k_2$. In this case, the kinetic scheme reduces to

$$\begin{array}{ccc} n_1^{\text{on}} & \overset{k_1}{\longleftrightarrow} & n_3^{\text{off}} \\ \alpha\updownarrow & & \updownarrow\alpha \\ n_2^{\text{on}} & \underset{k_2}{\longleftrightarrow} & n_4^{\text{off}} \end{array} \tag{22}$$

It follows that we can write

$$\mathbf{K} = \begin{pmatrix} -(k_1+\alpha) & \alpha & k_1 & 0 \\ \alpha & -(k_2+\alpha) & 0 & k_2 \\ k_1 & 0 & -(k_1+\alpha) & \alpha \\ 0 & k_2 & \alpha & -(k_2+\alpha) \end{pmatrix} \tag{23}$$

and

$$\xi = \begin{pmatrix} 1 \\ 1 \\ 0 \\ 0 \end{pmatrix} \tag{24}$$

The eigenvalues of the matrix $\mathbf{K}$ are $\{0,-2\alpha,-\kappa_+,-\kappa_-\}$, where $\kappa_\pm = k_1 + k_2 + \alpha \pm \gamma$ and $\gamma = \sqrt{\alpha^2+(k_1-k_2)^2}$. It follows that

$$\mathbf{P}^{\text{eq}} = \begin{pmatrix} 1/4 \\ 1/4 \\ 1/4 \\ 1/4 \end{pmatrix} \tag{25}$$

If we define $k(t) = k_{I(t)}$, where

$$\mathbf{k} = \begin{pmatrix} k_1 \\ k_2 \\ k_1 \\ k_2 \end{pmatrix} \tag{26}$$

it follows from eqs 7 and 8 that

$$\langle k(t)\rangle = \frac{1}{2}(k_1 + k_2) \tag{27}$$

and

$$\langle k(t)k(0)\rangle = \frac{1}{4}((k_1+k_2)^2 + (k_1-k_2)^2 e^{-2\alpha t}) \tag{28}$$

$k(t)$ represents the effective rate at any time t, since the system is in one of the four states, $I(t)$. The components of vector $\mathbf{k}$ define the rate constant associated with each state of the system. The fact that a nontrivial correlation exists here demonstrates how a Markovian scheme can generate an effective non-Markovian scheme when viewed as a collection of hidden states.

Here we see that the time dependence of the correlation function is consistent with the rate of transformation between the two schemes α. The following expressions for the correlation functions can be explicitly evaluated:

$$C_2(t) = \frac{e^{-\kappa_+ t}}{2\gamma}[\alpha(e^{2\gamma t} - 1) + \gamma(e^{2\gamma t} + 1)] \tag{29}$$

and

$$C_4(\tau,t) = \frac{1}{4\gamma^2} \left[\begin{array}{l} 2\alpha^2(e^{-2\kappa_+\tau} + e^{-2\kappa_-\tau}) - 2\alpha\gamma(e^{-2\kappa_+\tau} - e^{-2\kappa_-\tau}) \\ +(k_1-k_2)^2 e^{-2\alpha t - 2\kappa_+\tau}(2e^{2\gamma\tau}(e^{2\alpha t}-1)+(e^{4\gamma\tau}+1)(e^{2\alpha t}+1)) \end{array} \right] \tag{30}$$

The $r(m)$ of the 2×2 model will be simulated using a numeric approach to be described later.

Introduction of Continuous Stochastic Control Variables

A simple model of the statistical fluctuations of $k_{ij}(t)$ can be constructed by considering a set of stochastic control variables. We will denote them by $x(t)$ and assume that $k_{ij}(t)$ is defined parametrically through the dependence $k_{ij}(t) = F_{ij}(x(t))$, where $F_{ij}(x)$ is a specified function of the control variable x. We describe the motion of the control variable by a Langevin equation as used in Brownian motion theory,[20]

$$\frac{d}{dt}x(t) = -\lambda x(t) + f(t) \tag{31}$$

where $f(t)$ is a Gaussian random variable with white noise. $\langle f(t)\rangle = 0$ and $\langle f(t_1)f(t_0)\rangle = 2\lambda\theta\delta(t_1 - t_0)$ must be consistent with the fluctuation−dissipation theorem. It is possible to generate a characteristic stochastic trajectory $x(t)$ by numerically integrating this equation. We represent this as

$$dx(t) = -\lambda x(t)dt + \sqrt{2\theta\lambda}dw(t) \tag{32}$$

where $w(t)$ is a Wiener process[36−38] satisfying $\langle dw(t)dw(t)\rangle = dt$. For each t, dw can be viewed as an independent Gaussian random variable with variance dt. The conditional probability density for x, $P(x,t;x_0,t_0)$, satisfies the Fokker−Planck equation

$$\frac{\partial}{\partial t}P = \frac{\partial}{\partial x}(\lambda x P) + \lambda\theta\frac{\partial^2}{\partial x^2}P \tag{33}$$

This is an example where a Markovian process $dw(t)$ (Weiner) is used to generate a non-Markovian stochastic variable $x(t)$. With $x(t)$ characterized, we are in a position to incorporate these fluctuations in the kinetic model. The simplest way to achieve this is to modify the 1×2 model to include a time-dependent forward rate.

Diffusive Model

Consider the following two-state model with the stochastic rate constant, $k_{21}(t) = k_{21}^0 e^{-x(t)}$, where $x(t)$ is a stochastic control variable. Because the control variable at time t will be correlated with the value at time 0, the resulting dynamics will be non-Markovian by construction. The kinetic scheme for this system may be represented as

$$n_1^{\text{on}} \underset{k_{12}^0}{\overset{k_{21}^0 e^{-x(t)}}{\rightleftharpoons}} n_2^{\text{off}} \tag{34}$$

This scheme is called "diffusive" or "Agmon−Hopfield" dynamics.[21] The rate coefficient matrix can be written as

$$\mathbf{K} = \begin{pmatrix} -k_{21}^0 e^{-x(t)} & k_{12}^0 \\ k_{21}^0 e^{-x(t)} & -k_{12}^0 \end{pmatrix} \tag{35}$$

and the observable parameters are given by

$$\xi = \begin{pmatrix} 1 \\ 0 \end{pmatrix} \tag{36}$$

The control variable is described by a Gaussian random process characterized by zero mean, $\langle x(t)\rangle = 0$, and the correlation time $1/\lambda$ and strength θ:

$$\langle x(t)x(0)\rangle = \theta e^{-\lambda t} \tag{37}$$

It then follows that $k_{21}(t)$ is a Gaussian random process with

$$\langle k_{21}(t)\rangle = k_{21}^0 e^{1/2\theta} \tag{38}$$

and

$$\langle k_{21}(t)k_{21}(0)\rangle = (k_{21}^0)^2 e^{\theta(1+e^{-\lambda t})} \tag{39}$$

The corresponding $C_2(t)$, $C_4(\tau,t)$ and $r(m)$ will be numerically simulated. Here we see that the rate constant is correlated over a "continuum of time scales" because of the exponential of an exponential occurring in eq 39, in contrast to a few exponentionals for the 2×2 model.

Numerical Technique

Viewed as a Markovian process, the single molecule trajectory $I(t)$ is simulated using Monte Carlo simulation techniques. This is achieved by stepping in time in discrete steps of dt. At any point in time t, if the system is in the state i, the probability of making a transition to another state in time dt is $\Gamma_i dt$, where $\Gamma_i = \sum_{j\neq i} k_{ji}$. A decision to make a transition is determined from a uniformly distributed random number. Given that a transition has occurred, the probability for the new condition being j is k_{ji}/Γ_i. A uniformly distributed random number again determines the choice of this final state. This procedure generates a trajectory that has statistical time dependence consistent with that of the distribution given by eq 1.

The incorporation of time-dependent rate constants is straightforward. While we are stepping in time, we integrate the Langevin equations describing the time dependence of the control variables, $x(t)$ (see eq 31). From the characteristic trajectory, we are able to evaluate relevant correlation functions and averages. If we are interested in quantities that only involve $G_{ij}(t,t_0)$, it is possible to integrate the coupled set of equations, eqs 2 and 31, where the coupling occurs through the rate-constant dependence on $x(t)$.

Theoretical Results

We can now compare analytical and simulation results of the three models presented above. Our goal is to investigate the qualitative difference between these simple models in hope that through comparison to experiment, we will be able to distinguish between them.

Figure 1A and B shows the linear and logarithmic plots of the second-order correlation function of ξ, $C_2(t)$, for the 1×2, 2×2, and diffusive models. The $C_2(t)$ of the 1×2 model is a single-exponential decay (eq 19). While the 2×2 and the diffusive models clearly differ from the single exponential decay, the difference between the two is most obvious at long time intervals ($C_2(t) < 0.1$), as seen clearly in the log plot. We used $k_{21} = 1$ and $k_{12} = 1$ for the 1×2 model;. $k_1 = 2.0$, $k_2 = 0.4$, and $\alpha = 0.15$ for the 2×2 model; $\lambda = 0.25$ and $\theta = 0.5$ for the diffusive model. These parameters were chosen so that the decays would be on the same time scale. The multiexponential character of the diffusive model relative to the 2×2 model is evident here. To distinguish between the diffusive and 2×2 models it is necessary to have an accurate signal at longer times where the correlation has significantly diminished in value.

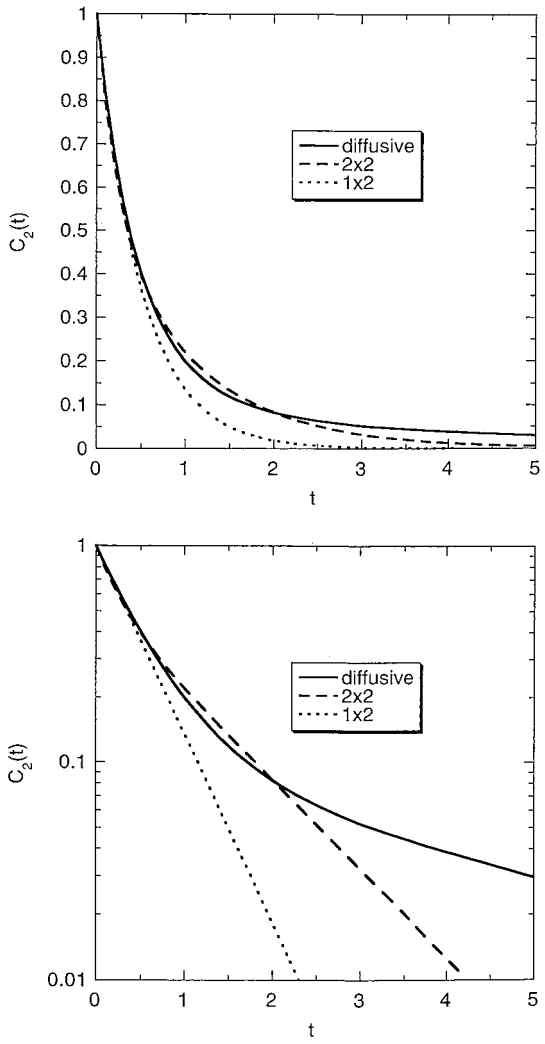

Figure 1. A. Linear plot of the calculated autocorrelation functions of $\Delta\xi$, $C_2(t)$, for the 1×2 model (dotted line, with $k_{21}^o = k_{12}^o = 1$), the 2×2 model (dashed line, with $k_1 = 2$, $k_2 = 0.4$, and $\alpha = 0.15$) and the diffusive model (solid line, with $k_{12}^o = k_{21}^o = 1$, $\lambda = 0.25$, $\theta = 0.5$). B. Logarithmic plot of the same $C_2(t)$.

In Figure 2A and B, we display the on-time autocorrelation function, $r(m)$ for the three models. $r(m)$ for 1×2 model is a spike at zero time. The two other models show similar dependence for the range of $0 \leq m \leq 2$, and differ at larger m. It would be difficult to distinguish between a 2×2 model and a diffusive model using this measure. The 1×2 model is easily distinguished from the others, clearly displaying the non-Markovian behavior.

Figure 3A and B shows the plots of the fourth-order correlation functions of ξ, $C_4(\tau,t)$, for the 2×2 model, as a function of τ for the values of $t = 0$, 0.5, 1.0, 1.5, and 2.0. Compare this to $C_4(\tau,t)$ for the 1×2 model, which is not dependent on t when $p = 0.5$. Figure 4A and B shows the plots

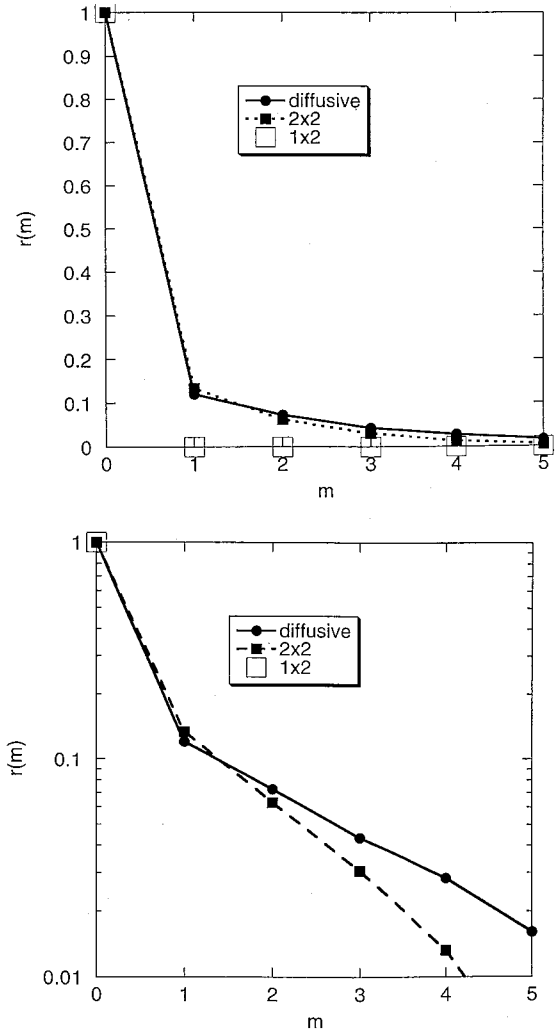

Figure 2. A. Linear plot of the simulated autocorrelation function of on-times, $r(m)$, as a function of turnover index number, m. The results are based on the 1×2 model (unfilled squares, a spike only at $m = 0$), the 2×2 model (black squares), and the diffusive model (round dots). B. Logarithmic plot of the same $r(m)$.

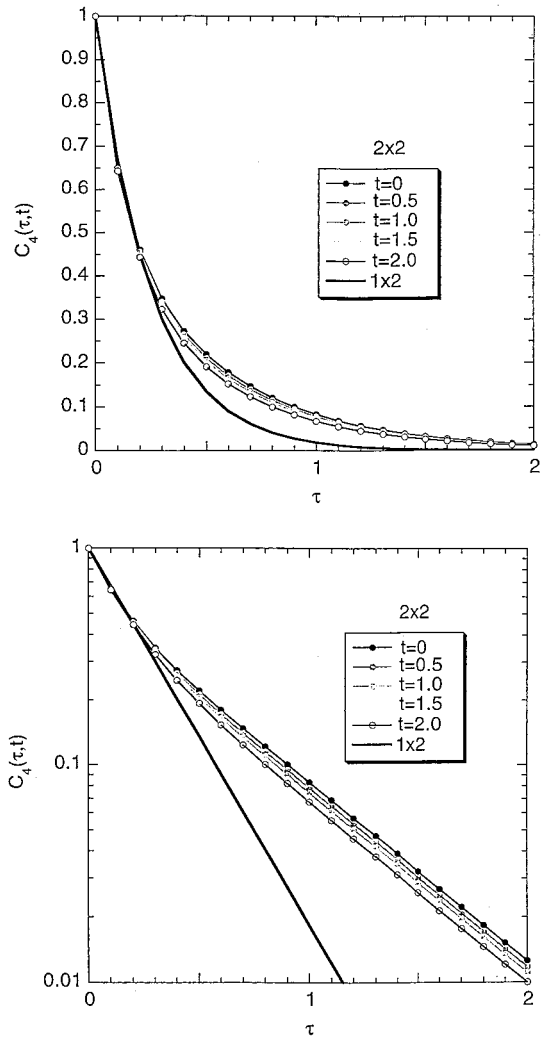

Figure 3. A. Linear plot of the simulated fourth order correlation functions of ξ, $C_4(\tau,t)$, as a function of τ for $t = 0$, 0.5, 1.0, 1.5, 2.0, derived from the 2×2 model. For comparison, the solid line shows the result of the 1×2 model. B. Logarithmic plot of the same $C_4(\tau,t)$.

of the $C_4(\tau,t)$ for the diffusive model, as a function of τ for the values of $t = 0$, 0.5, 1.0, 1.5, and 2.0. The t-independent $C_4(\tau,t)$ for the 1×2 model is also shown for comparison. A comparison of $C_4(\tau,t)$ of the 2×2 model and the diffusive model shows similar behavior, especially in the short time range where $C_2(t) > 0.1$. In the long time scale where $C_4(\tau,t) < 0.1$, we see significant differences in the qualitative t dependence of the two models.

From the results presented above, it is easy to identify the deviation from the simplest 1×2 model. Although the 2×2 model and the diffusive model appear to be similar on the coarse scale, they are significantly different on the fine scale, especially in a longer time scale. The time dependence of the diffusive model and the 2×2 model can be best seen with the t dependence of $C_4(\tau,t)$. We note that simulation of the 2×2 model is parameter dependent, and we have only taken an exemplary set of parameters. One can make the kinetic scheme more complex by having more channels (3×2 or 4×2 models). The more complex kinetics scheme will of course require more parameters. The 2×2 and the diffusive model demonstrate two limiting cases. The goal of the statistical analyses of the experimental trajectories is to gain understanding of qualitative features of the distribution of the conformational states pertinent to enzymatic reactions by verifying the validity of these models.

Experimental Results

We now briefly describe a single-molecule enzymatic turnover experiment. More detailed experimental descriptions have appeared elsewhere.[5] Cholesterol oxidase (CO_x) from *Brevibacterium sphaeroides* is a monomeric protein of 53 KDa that catalyzes the oxidation of cholesterol oxidase by oxygen. Flavin adenine dinucleotide (FAD) is the active site tightly bound to the center of the protein. The oxidized state of FAD absorbs at 450 nm and emits fluorescence peaked at 520 nm, whereas the reduced state of FAD is not fluorescent. During cholesterol oxidation in an enzymatic turnover cycle, FAD is first reduced to $FADH_2$, and then reoxidized by oxygen. The FAD switches between the oxidized form and the reduced form in each enzymatic turnover cycle described by the Michaelis−Menten mechanism:

$$\underset{\text{on}}{\text{E}-\text{FAD}} + \text{S} \underset{k_-}{\overset{k_+}{\rightleftharpoons}} \underset{\text{on}}{\text{E}-\text{FAD}\cdot\text{S}} \xrightarrow{k_{21}} \underset{\text{off}}{\text{E}-\text{FADH}_2} + \text{P} \quad (40a)$$

$$\underset{\text{off}}{\text{E}-\text{FADH}_2} + \text{O}_2 \underset{k'_-}{\overset{k'_+}{\rightleftharpoons}} \underset{\text{off}}{\text{E}-\text{FADH}_2\cdot\text{O}_2} \xrightarrow{k_{12}} \underset{\text{on}}{\text{E}-\text{FAD}} + \text{H}_2\text{O}_2 \quad (40b)$$

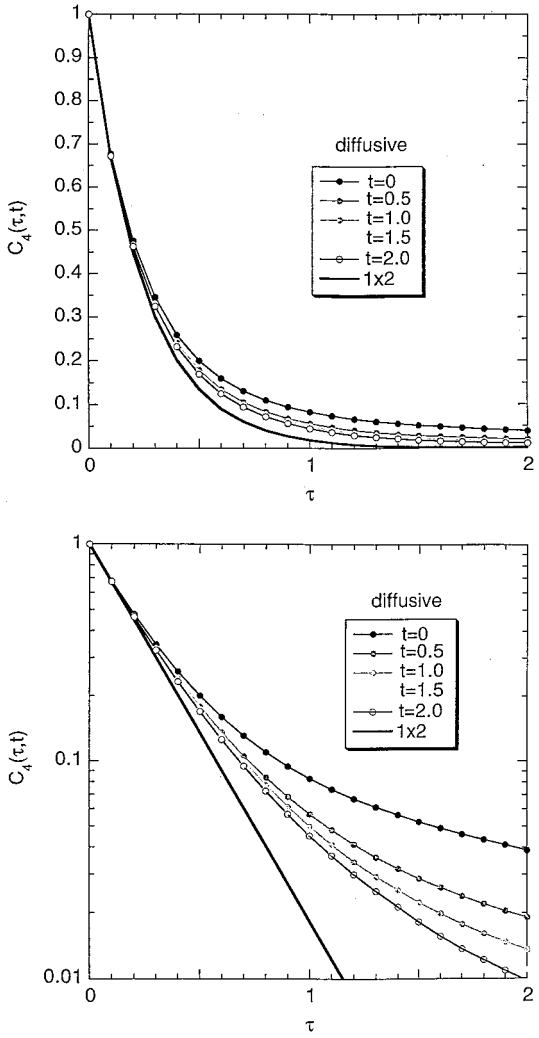

Figure 4. A. Linear plot of the simulated fourth order correlation functions of ξ, $C_4(\tau,t)$, as a function of τ for $t = 0$, 0.5, 1.0, 1.5, 2.0, derived from the diffusive model. For comparison, the solid line shows the result of the 1×2 model. B. Logarithmic plot of the same $C_4(\tau,t)$.

where S and P represent cholesterol substrate and oxidized product, respectively. The Michaelis−Menten mechanism has been recasted in terms of single-molecule kinetic analyses. The on- and off-time probability distributions have been derived for any substrate concentrations[5] k_{21}. The on- or off-time histograms are scrambled and less sensitive to dynamical fluctuations than correlation functions.

Under the condition that the concentration of the substrate is high, and/or the substrate is slowly reacting (such as 5-pregene-3β-20α-diol, a derivative of cholesterol) so that the activation steps (k_{21} and k_{12}) are rate limiting, the kinetic scheme reduces to the two-state (1×2) model in eq 17. This is the situation in which dynamical changes of protein conformation directly influence the activation of the enzymatic reaction, a situation on which we want to focus.

The CO_x molecules at low concentration (10^{-9} M) are confined in agarose gel containing 99% buffer solution containing 2mM of 5-pregene-3β-20α-diol. The COx molecules were tumbling freely, but the gel restricted their translational diffusion. The single-molecule enzymatic turnovers are observed in real time by monitoring the emission-intensity of the FAD in a single COx molecule.[5] Figure 5 shows a portion of a typical single COx emission-intensity trajectory. The trajectories were sufficiently long with more than 500 hundred turnovers, permitting detailed statistical analyses. The trajectories were converted to quantized data by removing the measurement noise. Correlation functions were derived from these filtered trajectories.

Figure 6A and B shows experimentally determined $C_2(t)$ of a COx molecule (molecule A). To compare the experimental data with the theoretical results, we must find the error bound in the measured correlation functions (dashed lines in Figure 6). It is important to note that the error bars result not from the measurement noise but from the finite lengths of trajectories. At short times, the error bars are smaller because of more averaging along the trajectory. In the appendix, we present the analytical expressions of the standard deviation (s.d.) of the correlation functions as a function of time that were used to generate the error bounds ($\pm$s.d.).

According to the simple two-state (1×2) model, a single-exponential decay (dotted line) is expected with a decay rate being the sum of the forward (k_{21}) and backward rates (k_{12}). However, we found that the measured $C_2(t)$ is clearly not single-exponential. The multiexponential decay of the autocorrelation function can arise from the dynamic disorder of k_{21} or k_{12}.

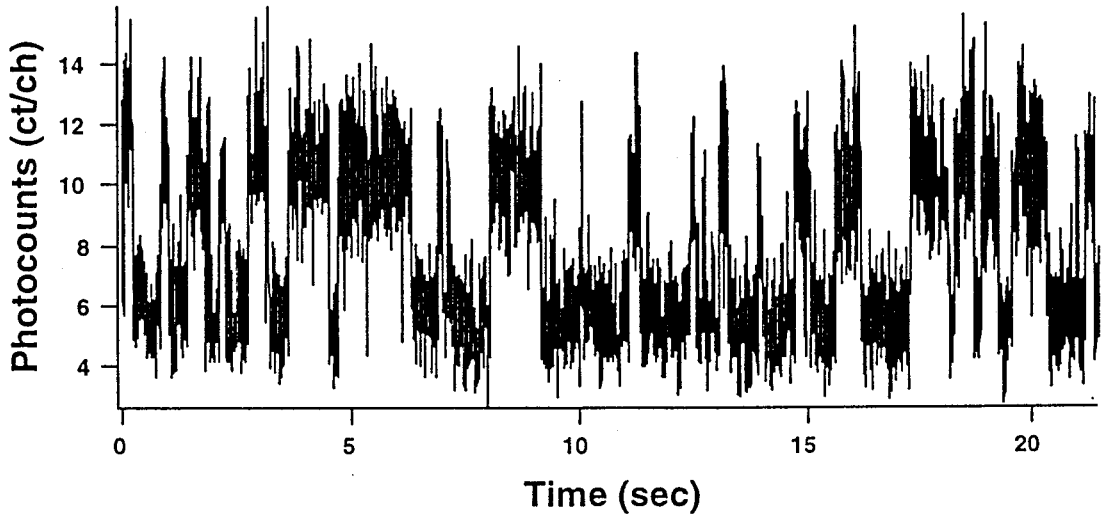

Figure 5. Real-time observation of enzymatic turnovers of a single CO_x molecule catalyzing oxidation of sterol molecules. This is a portion of an emission intensity trajectory recorded in 13.1 ms per data point. The emission exhibits stochastic blinking behavior as the active site FAD toggles between oxidized (fluorescent) and reduced (not fluorescent) forms, each on−off cycle corresponding to an enzymatic turnover. The substrate is cholesterol at 0.2 mM concentration. Quantized trajectories are obtained by removing the shot noise before correlation functions are evaluated.

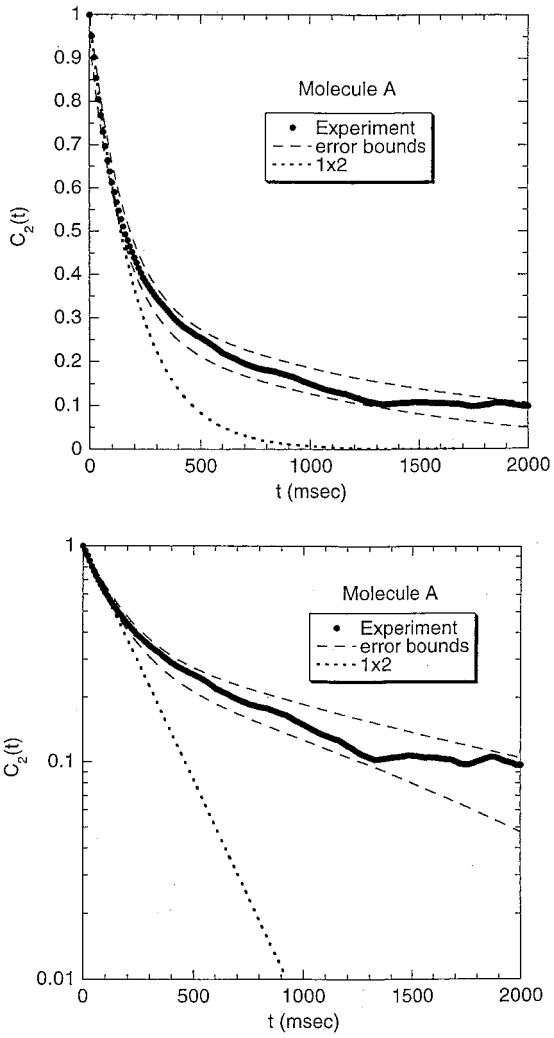

Figure 6. A. Molecule **A**'s $C_2(t)$ (dots) determined experimentally. The error bounds (dashed line) were obtained with the procedure in the Appendix. For comparison, the $C_2(t)$ of the 1×2 model is plotted on the same scale (dotted line). B. Logarithmic plot of the same $C_2(t)$.

To find out whether the dynamic disorder is in k_{21} or k_{12}, we evaluate the autocorrelation function, introduced previously,[5] of the on-times or off-times $r(m)$. The advantage of $r(m)$ of on-time (or off-time) is that it is only sensitive to forward (or backward) reaction. Figure 7 shows the $r(m)$ of molecule *A*'s on-times. If there is no dynamic disorder, $r(m)$ is expected to be only a spike at $m = 0$. The fact that $r(m) > 0$ at $m > 0$ indicates the fluctuation of k_{21}. In contrast, $r(m)$ for the off-time of molecule A (not shown) is a spike at $m = 0$, proving that there is no dynamic disorder for the backward reaction. The $r(m)$ in Figure 7 is similar to the simulated results in Figure 2. Although $r(m)$ is sensitive to identifying any non-Markovian behaviors, it is not particularly sensitive to distinguishing different models of dynamic disorder. Higher order correlation functions have the potential to distinguish different models.

Figure 8A and B shows the experimentally determined $C_4(\tau,t)$ of molecule A with its error bounds (see Appendix) for $t = 0$, clearly deviating from the 1×2 model. Figure 9 shows the t dependence of $C_4(\tau,t)$. For comparison, the $C_4(\tau,t)$ of the 1×2 model is also shown. The t dependence of $C_4(\tau,t)$ for the 1×2 model arises when the duty cycle of the trajectory is not 50% ($p = 0.25$ for molecule **A**) (eq 20). Simulations (Figures 3B and 4B) show that the $C_4(\tau,t)$ has stronger t dependence for the diffusive model than the 2×2 model. The experimental $C_4(\tau,t)$ is not capable of distinguishing between the two models.

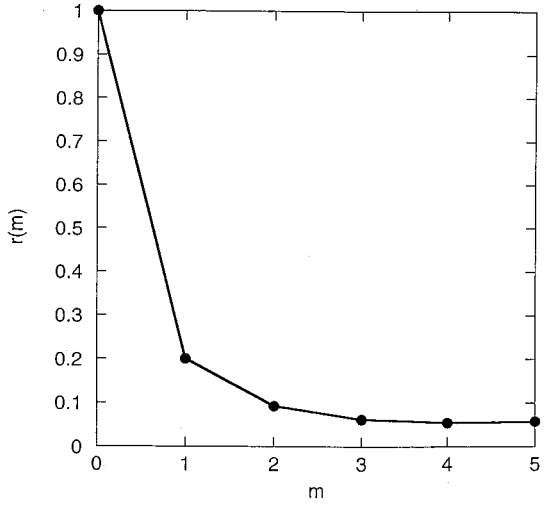

Figure 7. Molecule A's autocorrelation function of on-times $r(m)$ as a function of turnover index number m. This result proves that there is dynamic disorder in k_{21}.

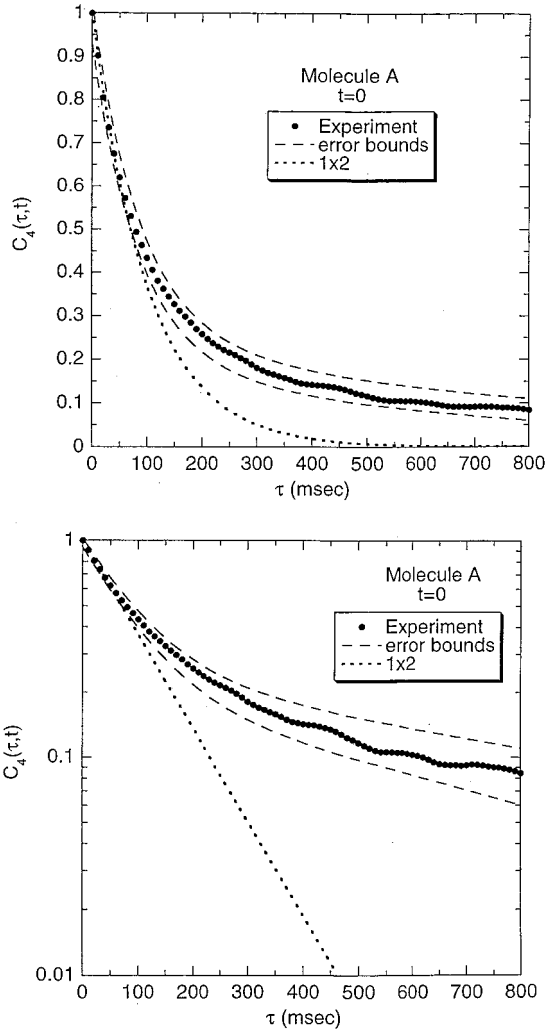

Figure 8. A. Molecule **A**'s $C_4(\tau,0)$ (dots) determined experimentally. The error bounds (dashed line) were obtained with the procedure in the Appendix. For comparison, the $C_4(\tau,0)$ of the 1×2 model is plotted on the same scale (dotted line). B. Logarithmic plot of the same $C_4(\tau,0)$.

Every molecule in the same system showed similar correlation functions, although we have observed static disorder.[5] For example, Figures 10 and 11 show the $C_2(t)$ and $C_4(\tau,t)$ at $t = 0$

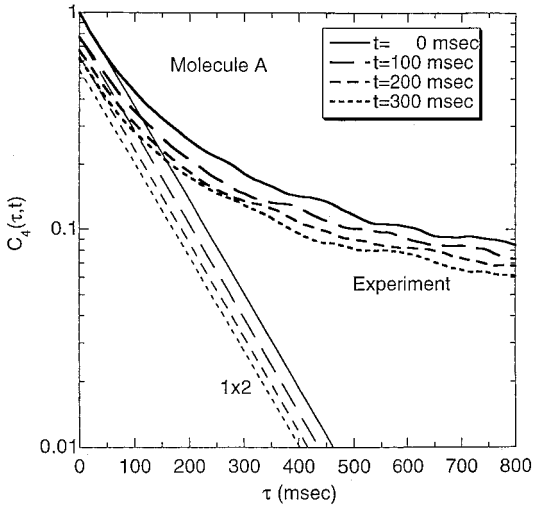

Figure 9. Logarithmic plot of molecule **A**'s $C_4(\tau,t)$ at $t = 0$, 100, 200, and 300 ms. simulations of $C_4(\tau,t)$ for the 1×2 model are also shown. The duty cycle of molecule **A** is $p = 0.25$.

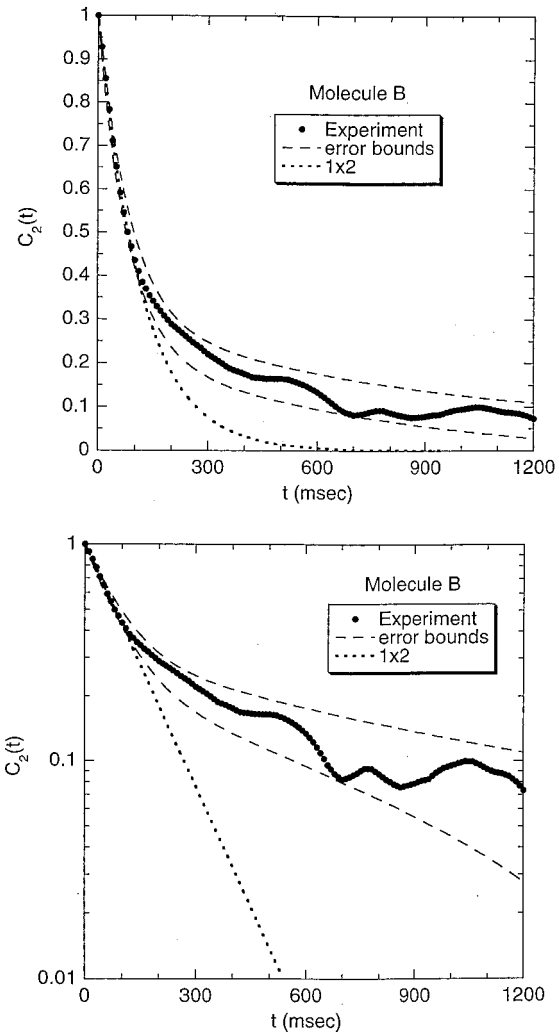

Figure 10. A. Molecule **B**'s $C_2(t)$ (dots) with error bounds(dashed lines). For comparison, the $C_2(t)$ of the 1×2 model is plotted on the same scale (dotted line). B. Logarithmic plot of the same. $C_2(t)$.

for molecule **B**, respectively. The error bounds are wider because of the shorter trajectory. Figure 12 shows the t dependence of $C_4(\tau,t)$ for molecule B. With the duty cycle close to 50% ($p = 0.45$), there is little t dependence for the 1×2 model.

TABLE 1: Resulting Values of χ^2 from Data Fitting

molecule	model	χ^2
A	2×2	0.479
A	diffusive	0.925
B	2×2	0.338
B	diffusive	0.432

TABLE 2: Fitted Rates for the 2×2 Model in Units of s^{-1}

	molecule	
	A	**B**
k_1	9.00	10.9
k_2	1.36	1.30
k'	1.03	4.43
α	0.130	0.610
β	0.0417	0.370

Fitting of Experimental Results

Having established the qualitative behavior of the C_2 and C_4 correlation functions corresponding to various models, in this section we demonstrate the ability to fit the experimental data directly. As a measure of fit, we define the goodness of fit parameter,

$$\chi^2 = \frac{1}{N_2}\sum_{i=0}^{N_2}(C_2^{\text{meas}}(i\Delta t_2) - C_2^{\text{model}}(i\Delta t_2))^2/\sigma_2^2(i\Delta t_2) + \frac{1}{N_{4\tau}N_{4t}}\sum_{i=0}^{N_{4\tau}}\sum_{j=0}^{N_{4t}}(C_4^{\text{meas}}(i\Delta\tau,j\Delta t) - C_4^{\text{model}}(i\Delta\tau,j\Delta t))^2/\sigma_4^2(i\Delta\tau,j\Delta t) \quad (41)$$

where the "meas" refers to measured to correlation functions determined from measured values, while the "model" refers to correlation functions determined from models. We take $N_2 = 200$, $\Delta t_2 = 10$ ms, $N_{4\tau} = 200$, $\Delta\tau = 10$ ms, $N_{4t} = 10$, and $\Delta t = 20$ ms. These values are chosen to cover the time range where the correction functions show significant structures. We consider three models whose parameters we adjust to minimize χ^2. The first is a 2×2 model of the form

$$\begin{array}{ccc} n_1^{\text{on}} & \overset{k_1}{\underset{k'}{\rightleftharpoons}} & n_3^{\text{off}} \\ \alpha\uparrow\downarrow\beta & & \alpha\uparrow\downarrow\beta \\ n_2^{\text{on}} & \overset{k_2}{\underset{k'}{\rightleftharpoons}} & n_4^{\text{off}} \end{array} \quad (42)$$

Here we set $k'_1 = k'_2 = k'$, corresponding to no dynamical disorder in the reverse reaction rate.

The next model is the diffusive model defined in the previous section by eq 34. Using an automated nonlinear least squares minimization algorithm for the finite 2×2 models, and varying parameters by hand to minimize χ^2 for the diffusive model, we find values for χ^2 displayed in Table 1. The corresponding parameters for the 2×2 model are displayed in Table 2, and for the diffusive model in Table 3.

For comparison, if we use a 1×2 model to fit the short time behavior of C_2 to determine κ and the measured value of $\langle\xi\rangle$ to determine an estimate of the forward and backward rate constants, we obtain a value of $\chi^2 = 23.95$ for molecule **A** and a value of $\chi^2 = 6.21$ for molecule B. The poor fit proves the presence of dynamic disorder.

For both molecules **A** and **B**, the 2×2 model generates significantly different k_1 and k_2 (more than factor of 5 difference). Similarly, the fittings with the diffusive model result in standard deviations of k_{21} being 110% and 190% of k_{21} for

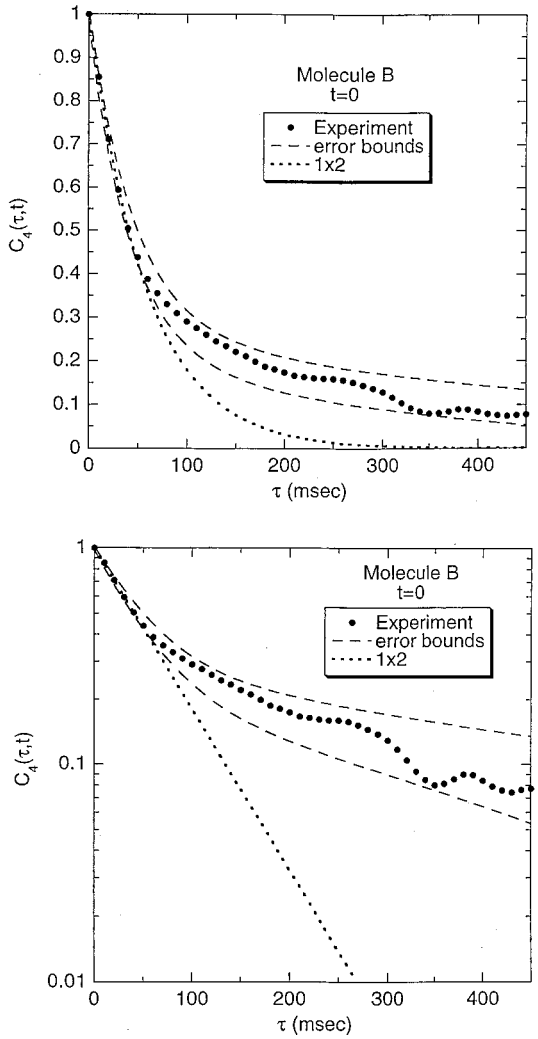

Figure 11. A. Molecule **B**'s $C_4(\tau,0)$ (dots) with error bounds (dashed lines). For comparison, the $C_4(\tau,0)$ of the 1×2 model is plotted on the same scale (dotted line). B. Logarithmic plot of the same $C_4(\tau,0)$.

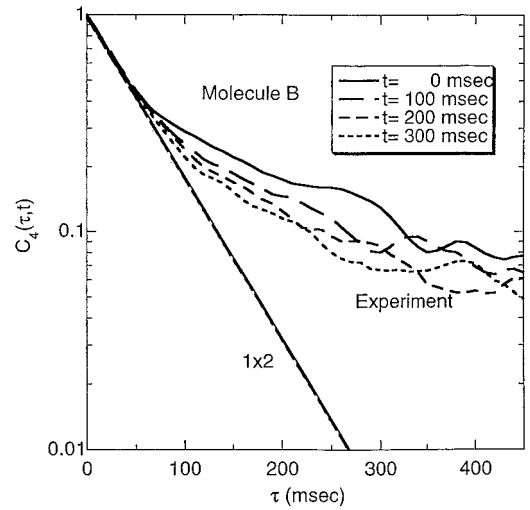

Figure 12. Logarithmic plot of molecule **B**'s $C_4(\tau,t)$ at $t = 0$, 100, 200, and 300 ms. Simulations of $C_4(\tau,t)$ for the 1×2 model are also shown. The duty cycle of molecule **B** is $p = 0.45$.

molecules **A** and **B**, respectively. The fittings show the significant influence of conformations on the rate of the activation step.

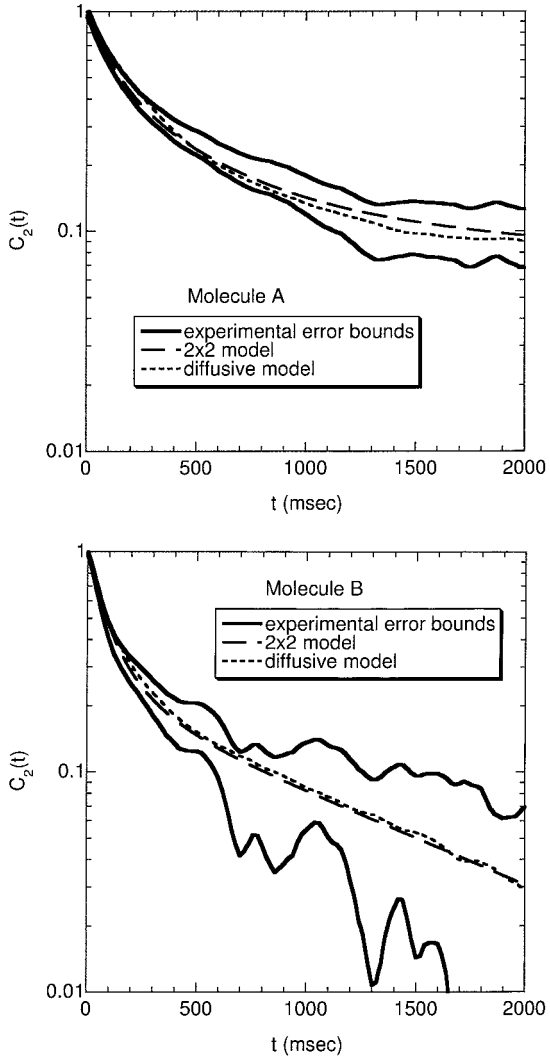

Figure 13. A. Logarithmic plot of the fitted $C_2(t)$ for molecule **A** based on the 2×2 and diffusive models. The error bounds are drawn from the experimental data plus/minus the standard deviation. Both models fit the data well. The fitted parameters are in Tables 2 and 3. B. The same for molecule **B**.

TABLE 3: Fitted Rates for the Diffusive Model in Units of s^{-1}

	molecule	
	A	B
k^0_{12}	1.20	4.73
k^0_{21}	3.80	3.87
λ	0.100	86.0
θ	0.80	1.50

We have also tried to fit the data with a 3×2 model:

$$\begin{array}{ccc} n_1^{\text{on}} & \overset{k_1}{\underset{k'}{\rightleftharpoons}} & n_4^{\text{off}} \\ \alpha\uparrow\downarrow\beta & & \alpha\uparrow\downarrow\beta \\ n_2^{\text{on}} & \overset{k_2}{\underset{k'}{\rightleftharpoons}} & n_5^{\text{off}} \\ \gamma\uparrow\downarrow\eta & & \gamma\uparrow\downarrow\eta \\ n_3^{\text{on}} & \overset{k_3}{\underset{k'}{\rightleftharpoons}} & n_6^{\text{off}} \end{array} \tag{43}$$

The 3×2 fits have $\chi^2 < 1$, similar to the situations of the 2×2 and diffusive models, but not significantly better. There is a large uncertainty of the fitted rate coefficients as expected.

With $\chi^2 < 1$ for both the 2×2 model and the diffusive models, fitted correlation functions fall well within the statistical error bars of the experimental correlation functions. This is graphically shown in Figures 13A and B. The fittings by both the 2×2 model and the diffusive model are equally good. Because of this, we cannot distinguish which model is more appropriate. To do so, we must have longer trajectories and/or more sophisticated analyses of trajectories.

Conclusions

The Michaelis−Menten mechanism, although correct in describing the averaged behaviors of large ensembles of molecules, does not provide a precise real-time picture on a single-molecule basis for cholesterol oxidase and perhaps other enzymes. Statistical analyses of the single-molecule measurement have revealed dynamic disorder in the rate of the activation step. This was attributed to slow conformational fluctuations otherwise hidden in conventional measurements done on large ensembles of molecules. Such a slow conformational fluctuation was also directly observed by spectral diffusion of the FAD on a similar time scale.[5]

We have presented a general methodology for simulating single-molecule trajectories with either Markovian or non-Markovian behavior. We have presented three theoretical models and relate them to the observables of single-molecule experiments. The simulations of correlation functions based on different models have been compared with the experimental results. The simple two-state model, corresponding to the Michaelis Menten mechanism with saturation of substrate, is inconsistent with the experimental observations. We conclude that there must be more than one conformer involved. It has been well established that proteins have many conformational substates.[40,41] The question is, what are the distribution of the functional important conformational states and the distribution of their rates? We have presented two non-Markovian models for two limiting cases, with either two conformations (2×2 model) or a continuous distribution of conformations (diffusive model). Although there are noticeable differences in the autocorrelation functions derived from the two models, we are not yet in a position to determine which one of the two models or an intermediate between the two models is the underlying mechanism. The answer to this issue requires longer trajectories and/or more sophisticated analyses of trajectories. For example, the replica correlation functions have been put forward for a similar purpose.[42]

The conformational fluctuations influencing the reaction rate can be either global protein conformational changes or local conformational changes at the active site. The microscopic details of the conformational states are unknown, except that the barrier heights between the states are relatively high (15−20 kcal/mol assuming an Arrhenius process). It is likely that these slow fluctuations might have physiological significance.[39] Single-molecule experiments and statistical analyses will provide highly detailed information of the dynamics and functions of enzymes.

Acknowledgment. We thank Peter Wolynes for helpful discussions and sending us preprints prior to publication. This work was performed under the auspices of the Division of Chemical Sciences, Office of Basic Energy Sciences, U.S. Department of Energy under Contract DE-AC06-76RLO 1830 with Battelle Memorial Institute, which operates the Pacific Northwest National Laboratory, a multiprogram national laboratory.

Appendix

Here we discuss how to obtain the error bounds for the experimentally determined $C_2(t)$ and $C_4(\tau,t)$. For a trajectory of $\xi(t)$ with a finite length of T, we estimate the two-time correlation function $F_2(t) = \langle\Delta\xi(t)\Delta\xi(0)\rangle$ and the four-time correlation function $F_4(\tau,t) = \langle\Delta\xi(2\tau + t)\Delta\xi(\tau + t)\Delta\xi(\tau)\Delta\xi(0)\rangle$ using the mean estimators:

$$\bar{F}_2(t) = \frac{1}{T-t}\int_0^{T-t} dt' \Delta\xi(t+t')\Delta\xi(t') \tag{44}$$

and

$$\bar{F}_4(t) = \frac{1}{T-2\tau-t}\int_0^{T-2\tau-t} dt' \Delta\xi(2\tau+t+t')\Delta\xi(\tau+t+t')\Delta\xi(\tau+t')\Delta\xi(t') \tag{45}$$

For the purpose of estimating the errors in these quantities, we consider the standard deviation of the mean given by

$$\sigma_2(t) = \sqrt{\frac{4\bar{S}_2(t)}{\kappa(T-t)}} \tag{46}$$

and

$$\sigma_4(\tau,t) = \sqrt{\frac{4\bar{S}_4(\tau,t)}{\kappa(T-2\tau-t)}} \tag{47}$$

for the two- and four-time correlation functions, respectively. In these expressions we define the variance estimators

$$\bar{S}_2(t) = \frac{1}{T-t}\int_0^{T-t} dt' \Delta\xi(t+t')^2\Delta\xi(t')^2 - \bar{F}_2(t)^2 \tag{48}$$

and

$$\bar{S}_4(\tau,t) = \frac{1}{T-2\tau-t}\int_0^{T-2\tau-t} dt' \Delta\xi(2\tau+t+t')^2\Delta\xi(\tau+t+t')^2\Delta\xi(\tau+t')^2\Delta\xi(t')^2 - \bar{F}_4(\tau,t)^2 \tag{49}$$

The expression for the standard deviation of the mean is dependent on the number of independent samples of $\xi(t)$ in the interval $(0,T-t)$ in the case of $F_2(t)$ and $(0,T-2\tau-t)$ in the case of $F_4(\tau,t)$. To estimate this quantity, we use a correlation time scale of $4/\kappa$, where κ is determined from the short time dependence of $\bar{F}_2(t)$. The number of independent samples is then given by $\kappa(T-t)/4$ for the case of $F_2(t)$, and $\kappa(T-2\tau-t)/4$ for the case of $F_4(\tau,t)$. The error bounds in Figures 6, 8, 10, and 11 were generated in this manner.

References and Notes

(1) Xie, X. S.; Trautman, J. K. *Annu. Rev. Phys. Chem*. **1998**, *59*, 441.
(2) Nie, S.; Zare, R. N. *Annu. Rev. Biophys. Biomol. Struct.* **1997**, *26*, 567.
(3) Moerner, W. E.; Orrit, M. *Science* **1999** *283*, 1670.
(4) Weiss, S. *Science* **1999**, *283*, 1676.
(5) Lu, H. P.; Xun, L.; Xie, X. S. *Science* **1998**, *282*, 1877.
(6) Reilly, P. D.; Skinner, J. L. *Phys. Rev. Lett.* **1993**, *71*, 4257.
(7) Reilly, P. D.; Skinner, J. L. *J. Chem. Phys.* **1994**, *101*, 959. Reilly, P. D.; Skinner, J. L. *J. Chem. Phys.* **1994**, *101*, 965.
(8) Ambrose, W. P.; Moerner, W. E. *Nature* **1991**, *349*, 225.
(9) Pfluegl, W.; Brown, F. L. H.; Silbey, R. J. *J. Chem. Phys.* **1998**, *108*, 6876. Brown, F. L. H.; Silbey, R. J. *J. Chem. Phys.* **1998**, *108*, 7434.
(10) Tanimura, Y.; Takano, H.; Klafter, J. *J. Chem. Phys.* **1998**, *108*, 1851. Zumofen, G.; Klafter, J. *Chem. Phys. Lett.* **1994**, *219*, 303.
(11) Edman, L.; Mets, U.; Rigler, R. *Exp. Technol. Phys.* **1995**, *41*, 157.
(12) Jia, Y.; Sytnik, A.; Li, L.; Vladimarov, S.; Cooperman, B. S.; Hochstrasser, R. M. *Proc. Natl. Acad. Sci. U.S.A.* **1997**, *94*, 7932.

(13) Geva, E.; Skinner, J. L. *Chem. Phys. Lett.* **1998**, *288*, 255.
(14) Kubo, R. In *Fluctuation, Relaxation and Resonance in Magnetic Systems*; Haar, D. T., Ed.; Oliver and Boyd: London, 1961; p 23.
(15) Berezhkovskii, A. M.; Szabo, A.; Weiss, G. H. *J. Chem. Phys.* **1999**, *110*, 9145.
(16) Sakamann, B., Neher, E., Eds.; *Single-Channel Recording*, 2nd ed.; Plenum Press: New York, 1995; pp 397−482.
(17) For a review, see Colquhoun, D.; Hawkes, A. G. In *Single-Channel Recording*, 2nd ed.; Sakamann, B., Neher, E., Eds.; Plenum Press: New York, 1995; pp 397−482.
(18) Wang, J.; Wolynes, P. *Phys. Rev. Lett.* **1995**, *74*, 4317. Wang, J.; Wolynes, P. *J. Chem. Phys*. **1998**, *110***,** 4812.
(19) Zeldovich, Y. B.; Ruzmaikin, A. A.; Sokoloff, D. D. *The Almighty Chance*; World Scientific: Singapore, 1990.
(20) Zwanzig, R. *Acc. Chem. Res.* **1990**, *23*, 148.
(21) Agmon, N.; Hopfield, J. J. *J. Chem. Phys.* **1983**, *78*, 6947.
(22) Sumi, H.; Marcus, R. A. *J. Chem. Phys.* **1985**, *84*, 4894.
(23) Bagchi, B.; Fleming, G. R.; Oxtoby, D. W. *J. Chem. Phys.* **1983**, *78*, 7375.
(24) Kramers, H. A. *Physica* (Amsterdam) **1940**, *7*, 284.
(25) Straub, J. E.; Borkovec, M.; Berne, B. J. *J. Chem. Phys.* **1986**, *84*, 1788.
(26) Hanggi, P.; Talkner, P.; Borkovec, M. *Rev. Mod. Phys.* **1990**, *62*, 251.
(27) Pollak, E. In *Activated Barrier Crossing*; Hanggi, P.; Fleming, G., Eds.; World Scientific: Singapore, 1992.
(28) Tucker, S. C. In *New Trends in Kramers Reaction Rate Theory: Understanding Chemical Reactivity*; Talkner, P., Hanggi, P., Eds.; Kluwer Academic: Dordrecht, 1995.
(29) Grote, R. F.; Hynes, J. T. *J. Chem. Phys.* **1980**, *73*, 2715. Grote, R. F.; Hynes, J. T. *J. Chem. Phys.* **1981**, *74*, 4465. Grote, R. F.; Hynes, J. T. *J. Chem. Phys.* **1982**, *77*, 3736.
(30) Karplus, M. In *Femtochemistry and Femtobiology: Ultrafast Reaction Dynamics at Atomic-Scale Resolution, Nobel Symposium* 101; Sundstrom, V., Ed.; Imperial College Press: London, 1997.
(31) McCammon, J. A.; Gelin, B. R.; Karplus, M. *Nature* **1977**, *267*, 585.
(32) Bergsma, J. P., Hynes, T.; Reimers, J. R.; Wilson, K. R. *J. Chemi. Phys.* **1986**, *85*, 5625. Bergsma, J. P.; Gertner, B. J.; Wilson, K. R.; Hynes, J. T. *J. Chem. Phys.* **1987**, *86*, 1356. Wilson, K. R. In *Chemical Reactivity in Liquids: Fundamental Aspects*; Moreau, M.; Turq, P., Eds.; Plenum Publishing Co.: New York, 1988; p 231.
(33) Neria, E.; Karplus, M. *Chem. Phys. Lett.* **1997**, *267*, 23−30.
(34) Gehlen, J. N.; Marchi, M.; Chandler, D. *Science* **1994**, *263*, 499.
(35) Hoffman, B. M.; Ratner, M. A. *J. Am. Chem. Soc.* **1987**, *109*, 6237.
(36) Weiss, G. H. *Stat. Phys.* **1972**, *6*, 179.
(37) van Kampen, N. G. *Phys. Rep.* **1985**, *124*, 69.
(38) Arnold, L.*Stochastic Differential Equations: Theory and Applications*; Wiley: New York, 1974.
(39) Xie, X. S.; Lu, H. P. *J. Bio. Chem.* **1999**, *274*, 15967.
(40) Frauenfelder, H.; Sligar, S. G.; Wolynes, P. G. *Science* **1991**. *254*, 1598.
(41) Hagen, S. J.; Eaton, W. A. *J. Phy. Chem.* **1996**, *104*, 3395.
(42) Onuchic, J. N.; Wang, J.; Wolynes, P. G. *Chem. Phys.* **1994**. In press.